

PAPER • OPEN ACCESS

Analysis of preparatory directional solidification experiments for a new X-ray facility for the International Space Station

To cite this article: G. Reinhart et al 2025 IOP Conf. Ser.: Mater. Sci. Eng. 1335 012003

View the <u>article online</u> for updates and enhancements.

You may also like

- The effects of scrap addition on the structure and precipitation hardening of hypereutectic Al-Fe alloys
 Suwaree Chankitmunkong, Tawatchai Tangsuksan, Anastasia V. Tyurnina et al.
- <u>Suppression of Dynamic Nucleation by an Inert Atmosphere in Zr-2.5Nb-0.11O in ISS-EML</u>
- G.P. Bracker, S. Nell, M. Beckers et al.
- Importance of buoyancy flow in the macrosegregation formation during solidification of VAR process Chenbo Xu, Haijie Zhang, Christian Gomes-Rodrigues et al.



doi:10.1088/1757-899X/1335/1/012003

Analysis of preparatory directional solidification experiments for a new X-ray facility for the International Space Station

G. Reinhart^{1*}, F. Kargl², M. Becker², L. Sturz³, D. J. Browne⁴ H. Nguyen-Thi¹, A. Frutos Pastor⁵, A. Sgambati⁵, W. Sillekens⁶

- ¹ Aix-Marseille Univ, Université de Toulon, CNRS, IM2NP UMR 7334, 13397 Marseille, France
- ² Institut für Materialphysik im Weltraum, Deutsches Zentrum für Luft- und Raumfahrt (DLR), Köln 51170, Germany
- ³ Access e.V., Intzestraße 5, Aachen 52072, Germany
- ⁴ School of Mechanical and Materials Engineering, University College Dublin, Belfield, Dublin 4, Ireland
- ⁵ European Space Agency, ESTEC LEO Payload Team, Directorate of Human and Robotic Exploration; PO Box 299, 2200 AG Noordwijk, Netherlands
- ⁶ European Space Agency, ESTEC Utilisation and Enabled Science Team, Directorate of Human and Robotic Exploration; PO Box 299, 2200 AG Noordwijk, Netherlands

*E-mail: guillaume.reinhart@im2np.fr

Abstract. In the last decade, the use of X-ray radiography has been adapted to the study of solidification aboard microgravity platforms such as sounding rockets and parabolic flights. However, the limited microgravity duration accessible via these platforms is not sufficient to reach steady-state conditions. The European Space Agency (ESA) is currently developing a facility for the International Space Station (ISS) to overcome this limitation. Unlike the other microgravity platforms, XRF (X-Ray Facility) will enable multiple experiments so that statistical variations can be studied, and the principal parameters varied by design. The present contribution reports recent experimental investigations carried out on Earth using the "Experiment Unit 1" (EU-1) dedicated to the study of the directional solidification of aluminium alloys. While the objective of these activities was to validate the technical performance of the set-up, preliminary scientific insights were also gained. Information on the temperature field and grain structure formation is derived from analyses of image sequences and the possibilities offered by this new device are presented and discussed.

1. Introduction

A thorough understanding of complex phenomena acting at different scales in time and space is necessary to control solidification processes. Typical examples are grain nucleation, chemical diffusion, dendritic growth, fluid flow, and development of gas bubbles. Most of these phenomena are dynamic, and so in-situ and real-time observation techniques must be retained as methods of choice to carry out experimental investigations [1]. An additional challenge for the study of solidification is the occurrence of disturbing gravity-related effects on Earth, such as buoyancy-

Content from this work may be used under the terms of the Creative Commons Attribution 4.0 licence. Any further distribution of this work must maintain attribution to the author(s) and the title of the work, journal citation and DOI.

doi:10.1088/1757-899X/1335/1/012003

driven convection [2] and the sedimentation/flotation of solid grains and dendrite fragments [3]. These effects are well-known to significantly affect the grain structure formation and induce detrimental chemically segregated areas that are at the origin of critical defects such as cracks in industrially manufactured metal parts.

The recent development of powerful microfocus X-ray sources and modern X-ray detectors has enabled the application of laboratory X-ray radiography to directly visualise the solidification of metal alloys [4–6]. X-ray radiography systems have been successfully adapted into experimental devices used aboard microgravity platforms during the last decade [7,8]. Solidification experiments performed on parabolic flights [9,10] and sounding rockets [11–14] allowed benchmark data to be collected in purely diffusive conditions and highlighted the impact of gravity by comparison with ground experiments. However, the limited microgravity duration accessible via the latter platforms is not sufficient to reach steady-state conditions. Furthermore, only a small number of experimental conditions have been hitherto investigated due to the scarce opportunities to perform in-situ and time-resolved investigations of metal alloy solidification in a microgravity environment.

A way to overcome these limitations is the use of an experimental facility that can be operated on a space station. XRF (X-Ray Facility) is a device currently developed by ESA (European Space Agency) for ISS (International Space Station). Unlike the other microgravity platforms, XRF aims at enabling multiple experiments so that statistical variations can be studied, and the principal parameters varied by design. The experiment unit EU-1 is dedicated to the study of the directional solidification of aluminium alloys. Experimental investigations have been carried out on Earth to validate the technical performance of the set-up and preliminary scientific insights were also gained. Information on the temperature gradient evolution in the field of view was determined by two methods: (i) by marking the position of the eutectic isotherm during successive stabilisation periods at different temperatures and (ii) by measuring the eutectic front velocity during cooling. Solidification by sample pulling is also implemented and the possibilities offered by this feature are presented and discussed.

2. Experimental details

The X-Ray Facility (XRF) is developed in collaboration with Airbus Defence and Space and SSC (Swedish Space Corporation) and is based on a modular approach (Figure 1a). It consists of a core unit with a microfocus X-ray source and an experiment unit. The experiment unit EU-1 includes a furnace with crucible/sample and a detector enabling the real-time imaging of solidification for typically aluminium alloys.

2.1 Directional solidification apparatus

The gradient furnace is of Bridgman-Stockbarger type and is based on the XRMON-GF device previously developed by SSC in the framework of the ESA-XRMON project [8,15]. It has two identical heating elements separated by an adiabatic gap containing a 5 mm \times 5 mm window that constitutes the Field of View (FoV) through which the X-rays can pass. The two heating elements are controlled by two K-type thermocouples spaced d=14.4 mm apart. The temperature regulation enables controlled heating and cooling rates R within the range of 0.01 to 2 °C/s. An applied temperature gradient can be estimated by dividing the temperature difference between the hot side and the cold side by the distance between the thermocouples $G_{app} = (T_{hot} - T_{cold})/d$.

The heating elements can reach a maximum temperature of 900°C, which is sufficient to study the solidification of aluminium-based alloys provided that the difference in X-ray absorption

between the solid and the liquid phase is sufficient to obtain a good contrast. Tests have been hitherto successfully performed on Al-4wt.%Cu, Al-10wt.%Cu, Al-20wt.%Cu, and Al-49wt.%Ge. Here we will focus on representative observations obtained with a grain-refined Al-20wt.%Cu (Al-Ti-B) alloy. The sample dimensions were 50 mm in length, 5 mm in width and $200 \pm 10 \, \mu m$ in thickness and polished with 3 µm diamond paste. The sample length is chosen to obtain a sufficient heat flux from the hot to the cold side. The width allows a dendritic network to be observed. The thickness value is a compromise between having a good radiographic contrast, reducing convection effects, and avoiding the superimposition of several layers of dendrites, which would be detrimental to the picture legibility. The samples were sandwiched between two glassy carbon sheets sewn together with a silica thread whilst held in place in the middle of stainless-steel spacers. The holder/crucible/sample assembly was slid into the furnace and straddled both heating elements to achieve the expected thermal profile. It was then connected to a motorised translation device enabling a displacement of ± 10 mm from the centre of the furnace at velocities ranging from 0.1 to 100 µm/s. By this means, solidification can be achieved by concomitantly decreasing the heating element temperature at a given cooling rate, and/or by pulling the sample toward the cold zone of the furnace.

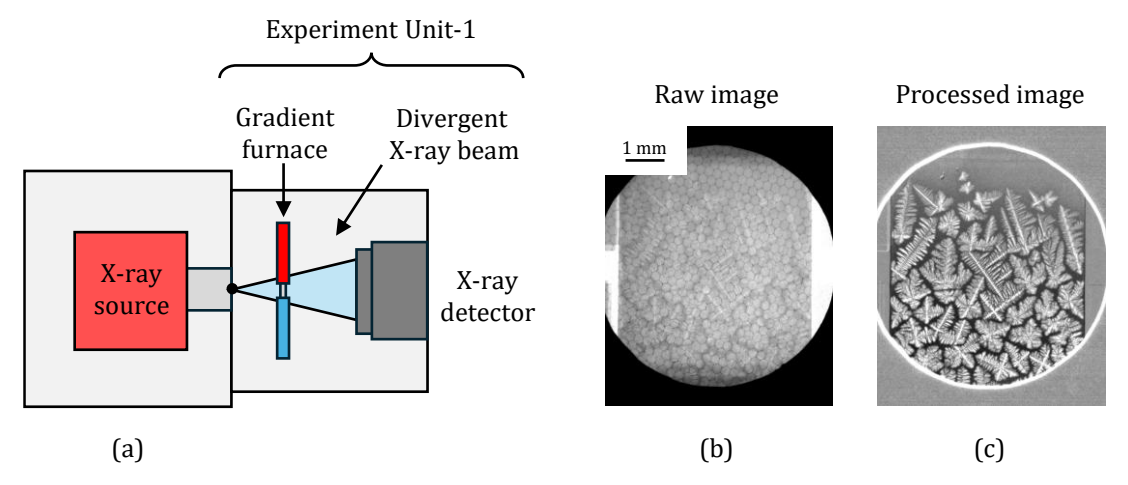


Figure 1. (a) Schematic illustration of XRF (X-Ray Facility) and experiment unit EU-1 dedicated to the study of the directional solidification of aluminium alloys. (b) raw radiograph and (c) processed image showing the grain structure formation for a refined Al-20wt.%Cu alloy ($G_{app} = 3$ °C/mm and R = -0.15 K/s).

2.2 Imaging system

The X-ray radiography device consists of a Hamamatsu L12531 micro-focus X-ray source [16] with a tungsten target generating a minimum spot size of 2 μm . The operating voltage and current used for the measurements were 60 kV and 100 μA , respectively. The detector system is a sCMOS 16MP_52 from Photonic Science [17]. The sensor has 4096 × 4096 pixels with a native pixel size of 9 μm . The X-ray source, furnace and detector were positioned so that an effective pixel size of 2 μm is obtained by geometrical magnification. The acquisition frequency was set to 2 frames per second, which was sufficient to follow the dynamics of the solidification microstructure formation and obtain images with a satisfactory signal to noise ratio.

doi:10.1088/1757-899X/1335/1/012003

A raw image recorded during the solidification of a refined Al-20wt.%Cu alloy is shown in Figure 1b. The honeycomb structure of the detector is visible and can be removed by image processing, either by applying a flat-field correction or by normalising the image recorded during solidification with an image recorded when the sample was fully liquid (Figure 1c). The solidifying dendritic grains are clearly distinguished in light grey, surrounded by solute-rich liquid in dark grey. In the following, the light grey regions corresponded to solid aluminium and the dark grey regions correspond to either solute-rich liquid or solid areas at the eutectic composition since the spatial resolution did not allow the two-phase eutectic structure to be distinguished.

3. Results and discussion

3.1 Temperature field characterisation

A major challenge during the investigation of solidification processes is to obtain reliable data on the temperature and temperature field in the sample, which is particularly important for further comparisons with numerical simulations. This is all the more difficult when using thin samples because putting a thermocouple in direct contact will interfere with the temperature field due to the heat flux along the wires which are not negligible compared to the heat flux through the sample, and therefore change the solidification conditions. Two methods have been devised during XRF tests campaigns, aiming at characterising the temperature field in the FoV when the sample is around the eutectic temperature. Both rely on the visualisation of the eutectic isotherm.

The first method takes advantage of the Temperature Gradient Zone Melting (TGZM) phenomenon, which has been studied in detail for instance by Nguyen-Thi et al. using postmortem investigations [18] and synchrotron radiography [19]. It consists in heating the solid sample in a temperature gradient until the melting of the eutectic phase surrounding the dendrites of the initial microstructure was detected in the top part of the FoV. Then the sample heating is stopped, and a stabilisation period of 10 to 15 minutes is applied. During the stabilisation period, an almost flat light-grey layer is formed just above the eutectic isotherm. The origin of this light-grey layer is the spontaneous migration of solute-rich liquid inclusions toward the hot part of the sample by TGZM. Consequently, the bottom part of the mushy zone becomes depleted in solute and consists only of solid aluminium in the whole thickness of the sample, clearly marking the position of the eutectic isotherm. Then, the temperature of both heating elements is raised by a value $\Delta T = 5^{\circ}C$ and a new stabilisation period is applied to induce the formation of a second aluminium-rich layer, below the first layer. This melting-stabilisation procedure is repeated several times until the eutectic isotherm reaches the bottom of the field-ofview, leaving behind consecutive light-grey lines indicating the previous positions of the eutectic isotherm, as shown by red arrows in Figure 2a.

The distance Δz between the position of two aluminium-rich layers at the end of their respective stabilisation period is then measured from the recorded images and the temperature gradient is estimated by using the relation $G = \Delta T/\Delta z$ (Figure 2a). This procedure was repeated until the eutectic isotherm reached the bottom of the FoV. The results are shown in Figure 2b for applied temperature gradients of 10 °C/mm (red circles) and 3 °C/mm (black squares) obtained by applying different temperature settings to the cold and hot side. In both cases, a gradual increase of G from the bottom to the top of FoV is obtained.

doi:10.1088/1757-899X/1335/1/012003

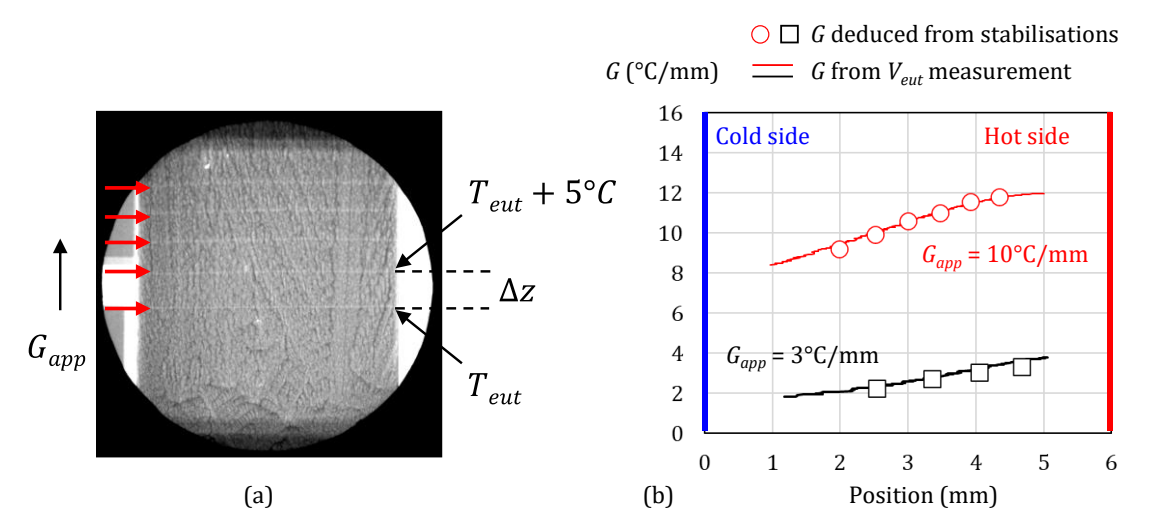


Figure 2. (a) Radiograph showing white aluminium-rich layers formed during successive stabilisation periods. (b) Temperature gradient measurements (refined Al-20wt.%Cu alloy, R = -0.15 K/s).

The second method consists of measuring the time evolution of the eutectic front position during directional solidification experiments when applying the same cooling rate on both heating elements. It is then possible to calculate the eutectic front velocity V_{eut} in the FoV and deduce the temperature gradient by using the relation $G=R/V_{eut}$, assuming that the cooling rate at the sample level is close to the one imposed on the heating elements, and that the eutectic front solidifies at a temperature close to the eutectic temperature. The results are also shown in Figure 2b for applied temperature gradients of 10 °C/mm (upper red line) and 3°C/mm (lower black line). A good agreement is obtained with the temperature gradient estimations determined by using TGZM, confirming the gradual increase of G from the bottom to the top of FoV.

It can be concluded that a comparable temperature field was equally obtained in static conditions during stabilisation or in dynamic conditions during cooling. It is worth noting that a similar gradual increase of *G* was also observed when investigating an Al-49wt.%Ge alloy. A possible origin for this behaviour can be an inherent asymetry of the heat flux related to the furnace design, such as heat loss at the empty window level in the adiabatic gap. Another possibility is the variation of solid and liquid fractions in the sample, which impacts the temperature gradient values since solid and liquid have different thermal conductivities. This effect has been investigated in detail for instance by Alkemper et al. [20] or Steinbach and Ratke [21] by using an aerogel furnace. Further experiments with a different cooling rate on the hot and cold heating elements would be necessary to determine the best way to compensate the temperature gradient change in the FoV.

It is also worth noting that the two presented methods only provide information on the temperature gradient at the eutectic temperature and that the corresponding temperature field cannot be directly transposed to the temperature field at a dendritic solidification front. However, a similar flatness of the isotherms and the highlighted increase in temperature gradient in the field of view should be qualitatively retrieved at the solidification front, as previously investigated by Soltani et al. [22] in a study on the impact of the temperature gradient on the equiaxed grain structure formation in Al-20wt.%Cu alloys.

doi:10.1088/1757-899X/1335/1/012003

3.2 Pulling experiment analysis

Only the solidification of the part of the sample in the FoV can be visualised when solidification is triggered by cooling down the heating element temperature. A way to follow the evolution of the solidification front over a longer distance is to pull the sample from the hot part to the cold part of the furnace. This possibility has been implemented in the current device, which enabled the investigation of the solidification front evolution over 20 mm of sample translation. The solidification front position was defined as the position of the leading dendrite tip (Figure 3a) and its evolution with time is reported in Figure 3b for a pull rate $V = -20 \,\mu\text{m/s}$.

A downward motion of the top of the mushy zone was observed during the stabilisation period before pulling (from 0 s to 225 s in Figure 3b). This behaviour is due to a flux of solute-rich liquid coming from the mushy zone by TGZM, which leads to a progressive increase of the liquid concentration at the top of the mushy zone and induces the dissolution of the solid. This phenomenon has also been reported and studied in detail for Al-4wt.%Cu alloys by using synchrotron imaging by Salloum et al. [23] and simulated by Phillion et al. [24] with a two-dimensional phase-field model and a volume averaged approach. The stabilisation was stopped when the top of the mushy zone reached approximately one third of the field of view, to have enough solid still visible to follow the microstructure evolution.

After pulling started, the solidification front first moved backward relative to the temperature gradient with a velocity equal to the pull rate. This front recoil has been analysed in detail by Warren and Langer [25] in the case of a planar front and reflects the time necessary for a solute layer to form above the solidification front due to solute rejection during solidification. A few seconds later, the solid-liquid interfaces underwent a Mullins-Sekerka instability [26] and dendritic microstructures started to develop. The solidification front moved upward and remained at a similar position (from 400 s to 720 s in Figure 3b). The peaks visible in the position curve are due to the successive nucleation of grains in the undercooled liquid that were eventually incorporated into the solidification front. The final upward motion (from 720 s to 900 s in Figure 3b) is most probably due to a change of the temperature field induced by a deformation of the upper part of the sample. This deformation occurred during the melting step because the liquid areas tend to contract due to surface tension and is exacerbated during the final stage of solidification due to sample shrinkage.

The sample was then remelted to perform further experiments. A drawback of sample cycling is that the solidified microstructure is erased during the melting step, preventing further postmortem analyses of the grain structure. A way to obtain an overview of the solidified grain structure is to create a composite image by stacking the parts of the images that went outside the FoV in between two frames during a pulling experiment. An example of such a reconstruction is shown in Figure 3c. The solidified grain structure can be clearly identified, showing the formation of large columnar grains. Most of the time the nucleated grains blocked the growth of the dendritic structure below but equiaxed grains can also be engulfed by the columnar front (yellow circle in Figure 3c). This behaviour is most probably related to a difference in grain competition with respect to the grain crystallographic orientations. Further systematic analyses would be necessary to better understand the mechanisms at the origin of this observation.

doi:10.1088/1757-899X/1335/1/012003

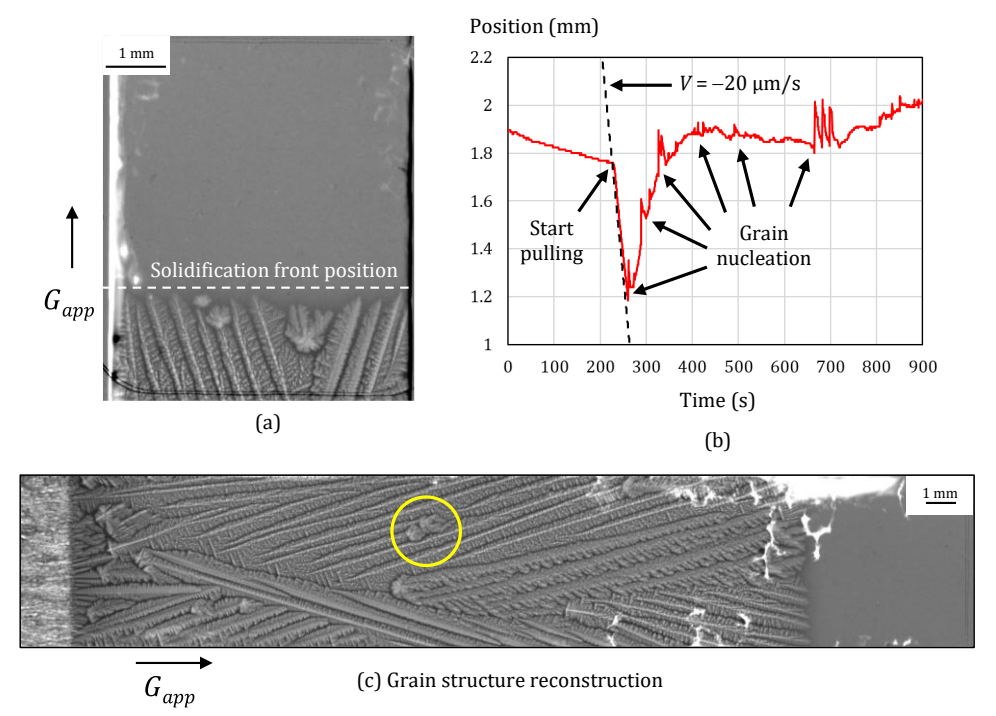


Figure 3. (a) Radiograph of the solidification front during a solidification by pulling experiment, (b) evolution of the solidification front position with time, and (c) composite image showing the solidified microstructure for a refined Al-20wt.%Cu alloy ($G_{app} = 10 \, ^{\circ}\text{C/mm}$ and $V = -20 \, \mu\text{m/s}$).

4. Conclusion

Preparatory experiments were conducted using XRF (X-Ray Facility) and the experiment unit EU-1 currently in development by ESA. The device has been successfully used to perform in-situ and time-resolved investigations of the directional solidification of aluminium alloys.

The collected data were used to characterise the temperature field in the FoV around the eutectic temperature. The analyses evidenced a gradual increase of the temperature gradient from the bottom to the top of the FoV. Further experiments are planned to investigate the means to reduce this effect. Ways of implementing thin thermocouples (<50 μ m) inside the crucible considering the limited space constraints of the device will also be investigated as a future work. Such experiments would also provide valuable information on the temperature field at the dendritic solidification front.

Solidification by pulling was successfully achieved, showing that the device enables the investigation of the solidification front dynamic until it reaches a quasi-steady state regime. An image processing was implemented to obtain an overview of the solidified grain structure before remelting of the sample.

The development of XRF/EU-1 is still ongoing, and this new platform is currently scheduled to be brought to ISS in Q1 2027.

References

- [1] Akamatsu S and Nguyen-Thi H 2016 Acta Mater. 108 325-46
- [2] Dupouy M D, Camel D and Favier J J 1993 Journal of Crystal Growth 126 480-92

- [3] Zimmermann G, Pickmann C, Hamacher M, Schaberger-Zimmermann E, Neumann-Heyme H, Eckert K and Eckert S 2017 *Acta Mater.* **126** 236–50
- [4] Rakete C, Baumbach C, Goldschmidt A, Samberg D, Schroer C G, Breede F, Stenzel C, Zimmermann G, Pickmann C, Houltz Y, Lockowandt C, Svenonius O, Wiklund P and Mathiesen R H 2011 *Rev. Sci. Instrum.* **82** 105108
- [5] Soltani H, Ngomesse F, Reinhart G, Benoudia M C, Zahzouh M and Nguyen-Thi H 2020 *Journal of Alloys and Compounds* 158028
- [6] Becker M, Kolbe M, Steinbach S and Kargl F 2022 Scripta Materialia 209 114386
- [7] Kargl F, Drescher J, Dreißigacker C, Balter M, Becker M, Wegener M and Sondermann E 2020 *Review of Scientific Instruments* **91** 013906
- [8] Reinhart G, Browne D J, Kargl F, García-Moreno F, Becker M, Sondermann E, Binder K, Mullen J S, Zimmermann G, Mathiesen R H, Sillekens W H and Nguyen-Thi H 2023 *npj Microgravity* **9** 1–10
- [9] Murphy A G, Li J, Janson O, Verga A and Browne D J 2014 *Materials Science Forum* **790–791** 52–8
- [10] Abou-Khalil L, Salloum-Abou-Jaoude G, Reinhart G, Pickmann C, Zimmermann G and Nguyen-Thi H 2016 *Acta Materialia* **110** 44–52
- [11] Nguyen-Thi H, Reinhart G, Salloum-Abou-Jaoude G, Browne D J, Murphy A G, Houltz Y, Li J, Voss D, Verga A, Mathiesen R H and Zimmermann G 2014 *Microgravity Sci. Technol.* **26** 37–50
- [12] Murphy A G, Mathiesen R H, Houltz Y, Li J, Lockowandt C, Henriksson K, Melville N and Browne D J 2016 *Journal of Crystal Growth* **454** 96–104
- [13] Ngomesse F, Reinhart G, Soltani H, Zimmermann G, Browne D J, Sillekens W and Nguyen-Thi H 2021 *Acta Materialia* **221** 117401
- [14] Becker M, Wegener M, Drescher J and Kargl F 2023 Metall Mater Trans A 54 4188–202
- [15] Nguyen-Thi H, Reinhart G, Salloum Abou Jaoude G, Mathiesen R H, Zimmermann G, Houltz Y, Voss D, Verga A, Browne D J and Murphy A G 2013 *Journal of Crystal Growth* **374** 23–30
- [16] https://www.hamamatsu.com/us/en/product/light-and-radiation-sources/microfocus-x-ray-source/L12531-01.html
- [17] https://photonicscience.com/products/x-ray-cameras/x-ray-scmos-16mp-detector/
- [18] Nguyen Thi H, Drevet B, Debierre J M, Camel D, Dabo Y and Billia B 2003 *Journal of Crystal Growth* **253** 539–48
- [19] Nguyen Thi H, Reinhart G, Buffet A, Schenk T, Mangelinck-Noël N, Jung H, Bergeon N, Billia B, Härtwig J and Baruchel J 2008 *Journal of Crystal Growth* **310** 2906–14
- [20] Alkemper J, Sous S, Stöcker C and Ratke L 1998 Journal of Crystal Growth 191 252-60
- [21] Steinbach S and Ratke L 2006 (https://publications.rwth-aachen.de/record/62189)
- [22] Soltani H, Reinhart G, Benoudia M C, Ngomesse F, Zahzouh M and Nguyen-Thi H 2022 Journal of Crystal Growth **587** 126645
- [23] Salloum-Abou-Jaoude G, Reinhart G, Combeau H, Založnik M, Lafford T A and Nguyen-Thi H 2015 *Journal of Crystal Growth* **411** 88–95
- [24] Phillion A B, Založnik M, Spindler I, Pinter N, Aledo C-A, Salloum-Abou-Jaoude G, Nguyen Thi H, Reinhart G, Boussinot G, Apel M and Combeau H 2017 *Acta Materialia* **141** 206–16
- [25] Warren J A and Langer J S 1993 Phys. Rev. E 47 2702-12
- [26] Mullins W W and Sekerka R F 1964 Journal of Applied Physics 35 444-51

Acknowledgements

This research is supported by the French National Space Agency (CNES) no. 200761/00 through the GDR MFA (no. 2799) network.